RSC Advances

PAPER

View Article Online
View Journal | View Issue

Cite this: *RSC Adv.*, 2020, **10**, 29181

Synthesis of 2D cobalt oxide nanosheets using a room temperature liquid metal†

Jessica Crawford,[ab] Aidan Cowman[b] and Anthony P. O'Mullane *[ab]

Received 10th July 2020
Accepted 30th July 2020

DOI: 10.1039/d0ra06010k

rsc.li/rsc-advances

Room temperature liquid metals based on Ga can be used as a synthesis medium for the creation of metal oxide nanomaterials, however one thermodynamic limitation is that metals that are more easily oxidised than Ga are required to ensure their preferential formation. In this work we demonstrate a proof of principle approach whereby exposing the liquid metal alloyed with the required metal to acidic conditions circumvents preferential formation of Ga_2O_3 and allows for the formation of the required 2D transition metal oxide nanosheets. The synthesis procedure is straightforward in that it only requires bubbling oxygen gas through the liquid metal alloy into a solution of 10 mM HCl. We show that the formation of thin nanosheets of *ca.* 1 nm in thickness of CoO is possible. The material is characterised using transmission electron microscopy, atomic force microscopy, X-ray photoelectron and Raman spectroscopy. The electrocatalytic activity of the CoO nanosheets was investigated for the oxygen evolution reaction where the nanosheet thickness was found to be a factor influencing the activity. This proof of principle offers a route to the possible formation of many other 2D transition metal oxides from metals that are less readily oxidised than Ga by taking advantage of the interesting properties of room temperature liquid metals.

Introduction

Galinstan is a eutectic alloy made from gallium, indium and tin with the ratio (Ga : 68.5%, In : 21.5%, Sn : 10%) that is a liquid at room temperature. Recently it has received significant attention due its physical and chemical properties and has been identified as an emerging material in nanotechnology[1–3] while being studied for many applications including use as a conductive ink,[4] stretchable and self-healing wires,[5] soft matter circuitry,[6] actuators,[7–11] and energy storage.[12] Recent work has shown that Ga based liquid metals can also be used as a solvent for the synthesis of a wide range of nanomaterials *via* chemical reactions that occur at the surface of the liquid metal under a variety of conditions including galvanic exchange at the surface of large liquid metal droplets or under sonication conditions which leads to composites containing gold that are catalytically active,[13] metal oxides such as MnO_2 that have photocatalytic properties,[14] Prussian blue nanomaterials,[15] as well as the ability to polymerise materials around the surface of liquid metal droplets.[16–18] One aspect that always needs to be considered when using galinstan, EGaIn or Ga in the liquid form is that when these materials are exposed to an oxygen containing atmosphere they spontaneously form a self limiting ~0.7 nm layer of Ga_2O_3 around the outside of the droplet, even when containing additional In or Sn components.[19] This phenomenon can be explained by calculation of the Gibbs free energy of formation (ΔG_f) of gallium oxide which is much lower than In_2O_3 or SnO_2 which therefore results in preferential formation of Ga_2O_3 at the surface. This phenomenon is also evident when other transition metals are incorporated in liquid metal galinstan such as Gd, Al or Hf. The Gibbs free energy of formation for Gd_2O_3 (−1732.3 kJ mol^{-1}), Al_2O_3 (−1582.3 kJ mol^{-1}) and HfO_2 (−1088.2 kJ mol^{-1}) are lower than Ga_2O_3 (−998.3 kJ mol^{-1})[20] which implies that these oxides would preferentially form over Ga_2O_3 to ensure the maximum reduction in the Gibb's free energy of the system. This was exploited in previous work where Gd_2O_3, Al_2O_3 and HfO_2 were expelled from the surface of galinstan into water *via* purging oxygen gas through a reservoir of liquid metal that contained the relevant metal to form atomically thin nanosheets.[21] With this approach many 2D transition metal oxide materials can in principle be produced as long as the incorporated metal is more readily oxidised than Ga.

Nanostructured transition metal oxides have shown excellent activity for many electrocatalytic reactions including those associated with water splitting, *i.e.* the hydrogen evolution reaction (HER) and the oxygen evolution reaction (OER). The OER has received particular attention given the sluggish kinetics of the process which limits overall performance for

[a]*School of Chemistry and Physics, Queensland University of Technology (QUT), Brisbane, QLD 4001, Australia. E-mail: anthony.omullane@qut.edu.au*

[b]*Centre for Materials Science, Queensland University of Technology (QUT), Brisbane, QLD 4001, Australia*

† Electronic supplementary information (ESI) available: AFM images, OER activity of aged samples, electrochemical surface area measurements. See DOI: 10.1039/d0ra06010k

electrochemical water splitting. Many transition metal oxides based on Fe, Co, Ni and Mn have been studied for alkaline electrolysis and several comprehensive reviews are available in this area.[22–26] The realisation of ultrathin nanosheets of such oxides is attractive for exposing edge sites and increasing the amount of active sites available for the reaction which is highly important in the development of new electrolysers for the generation of green hydrogen. At present there is an urgent need to replace currently used expensive precious metal oxide electrocatalysts and promisingly previous work has shown that cobalt oxide/hydroxide materials in particular show activity for the sluggish OER.[27–32]

In this work we extend the applicability of nanosheet formation from Ga based liquid metals by producing 2D nanosheets of a material that is unfavoured, namely oxidised Co (ΔG_f for CoO is -214.2 kJ mol^{-1} which is significantly higher than that for Ga_2O_3), *via* control of the solution pH into which the material is ejected. This material is then investigated for the OER under alkaline conditions.

Experimental

Materials

Cobalt powder 2 μm particle size (99.8%), Galinstan (gallium (68.5%) indium (21.5%) and tin (10%)) eutectic alloy and hydrochloric acid 37% were purchased from Sigma Aldrich. NaOH was purchased from Chem Supply. Ultra High Purity Oxygen was purchased from Supagas. Lacey Carbon copper coated TEM grids and silicon wafers were purchased from Ted Pella.

Methods

Synthesis of 2D CoO. 0.5, 1 and 1.5 wt% cobalt powder was mixed thoroughly into Galinstan on a glass slide for 20 minutes to ensure complete mixing. Once mixed, 0.5 g of this sample was transferred to a 1.5 mL centrifuge tube using a syringe, with 0.5 mL of a varied concentration (1, 10, 50 mM) of hydrochloric acid. A needle was inserted into the bottom of the centrifuge tube into the Co-Galinstan droplet as an inlet of O_2 gas. O_2 was flowed through the needle for 30 minutes.

Electrochemical measurements. The solution was allowed to settle to remove any potential liquid droplets in solution or larger particles. 5 μL was then taken and dropcast onto a glassy carbon (GC) electrode (3 mm diameter BASi). Prior to modification the GC electrode was polished on a Microcloth using 0.3 μm alumina particles, washed with MilliQ water and blown dry with a stream of nitrogen. After drop casting the sample the electrode was placed into an oven at 70 °C for 15 minutes. The material was tested as an electrocatalyst in a 3 electrode electrochemical cell set-up with a leakless Ag/AgCl reference electrode and a Pt wire counter electrode in 0.1 M NaOH electrolyte. The data was collected at a sweep rate of 20 mV s^{-1} using a Bio-Logic VMP3B-20 potentiostat. For the long term stability test the current density was set to 10 mA cm^{-2}. The data is given *versus* the RHE reference electrode *via* the following:

$$E_{RHE} = E_{Ag/AgCl} + 0.059 \times pH + E^0_{Ag/AgCl}\ V.$$

Material characterisation. The sample was dropcast onto a silicon wafer and measured using a Renishaw inVia Raman Microscope with a 735 nm laser at 10% capacity. X-ray Photoelectron spectroscopy data was collected using an Omicron Multiscan Lab Ultra-high Vacuum Scanning Tunnelling Microscope (UHV-STM) where a 125 mm hemispherical energy analyse was incorporated. Non-monochromatic Mg Kα (1253.6 eV) X-ray source was 1.0×10^{-9} Torr and the pressure was 1.0×10^{-8} during the experiment.

Samples were imaged using a Zeiss Sigma Scanning Electron Microscope. A JEOL 2100 transmission electron microscope was also used where the material was drop cast onto a lacey carbon copper TEM grid. Images were taken at 200 kV using diffraction mode with a selected area aperture to take diffraction patterns. A Bruker Atomic Force Microscope (AFM) using ScanAsyst in air method in contact mode was used to measure the thickness of samples. Gwyddion AFM analysis software was used to treat images and analyse all thicknesses. For every thickness measurement the mean from the low area and high area was taken and the difference calculated and rounded to 1 decimal point.

Results and discussion

The method used to produce 2D nanosheets from a liquid metal precursor is simple to set up and consists of an inlet tube allowing oxygen gas to flow through a reservoir of liquid Galinstan that is mixed beforehand with Co metal (0.5 to 1.5 wt%) for 30 min. The oxygen gas flows through the liquid metal causing disruption of the surface and expulsion of the outermost layers into an aqueous solution as shown in Fig. 1.

Our initial experiments were conducted with MilliQ water as the solvent using 0.5 wt% Co in Galinstan. As anticipated we did

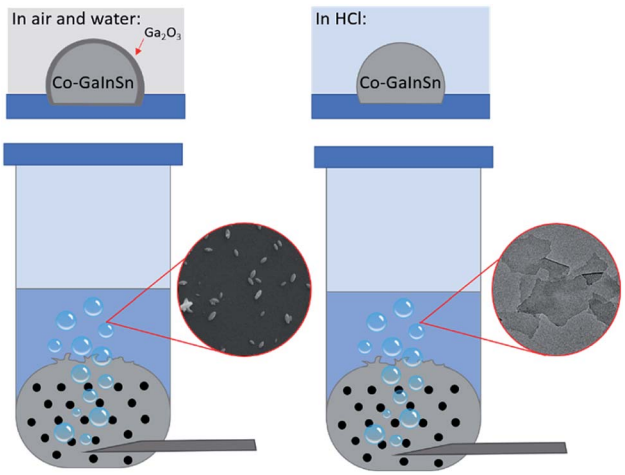

Fig. 1 The gas injection method showing Co–GaInSn in water forming gallium oxide and Co–GaInSn in hydrochloric acid forming cobalt oxide nanosheets.

not observe the formation of any Co containing species but saw an abundance of ellipsoid shaped particles generated in water when imaged by SEM (Fig. 2a) which are consistent with the formation of Ga oxides.[33–35] It is known that gallium oxides are soluble in acidic solution[36] and therefore the pH of the solution was controlled *via* the addition of HCl at various concentrations to minimise its formation. When the solution was acidified using 10 mM HCl there was a clear change in the morphology of the material ejected from the liquid metal (Fig. 2b and c). The formation of thin nanosheets can be observed (Fig. 2b) with some areas showing multiple sheets on top of each other or folded sheets (Fig. 2c). It should be noted that the sample was allowed to settle prior to analysis to remove any residual droplets that may have formed in the supernatant.

Electron diffraction measurements indicated that the material is amorphous (Fig. 2b inset). The individual sheets can be up to 500 nm in length whereas the folded sheets are larger. The thickness of the sheets was measured by atomic force microscopy (AFM) where an individual sheet is shown in Fig. 2d. The thickness of 50 different sheets was then measured and the histogram showing the distribution in thickness values (Fig. 2e) indicates that the sheets show that a high proportion are *ca.* 1 nm thick, indicating 2D nanosheet formation, with very few sheets as thick as 4.5 nm. The latter observation is due to the presence of sheets on top of each other or folded sheets as seen in the TEM images (Fig. 2c).

Raman spectroscopy was then undertaken and a typical Raman spectrum of the 2D nanosheets is shown in Fig. 3a. The peaks at (195.7, 619.7), 484.3 and 691.8 cm^{-1} can be assigned to the F_{2g}, E_g and A_{1g} active modes of CoO respectively.[37] The intense sharp peaks at 516.1 and 526.6 cm^{-1} are due to the underlying Si substrate that was used for AFM imaging purposes. X-ray photoelectron spectroscopy (XPS) analysis confirmed the formation of CoO. The Co 2p spectrum (Fig. 3b) can be fitted to the Co^{2+} oxidation state while the spin orbit splitting of 15.5 eV is also indicative of Co^{2+}.[38] The O 1s spectrum shows a peak at 531.8 eV which is generally consistent with the presence of hydroxide groups,[39] however there have been many reports which show that CoO nanomaterials exhibit a O 1s peak at a higher binding energy of 531.2 eV.[40,41] In particular it has been reported that this higher binding energy peak for CoO compared to that normally seen for lattice oxygen is due to a large number of defects which is encountered in very thin films.[40] It should also be noted that there was no evidence of gallium in the sample when analysed using XPS.

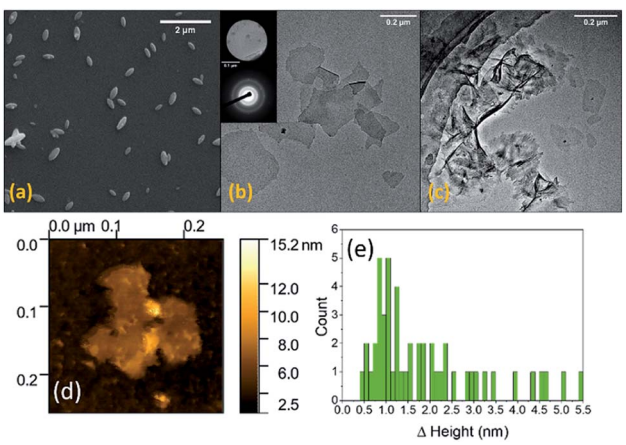

Fig. 2 (a) SEM image of gallium oxide formed in water, (b and c) TEM images of nanosheets formed from 0.5% Co–GaInSn in 10 mM HCl (inset of (b) shows the selected area electron diffraction pattern), (d) AFM image of an individual sheet and (e) histogram showing the measured thickness of 50 different sheets.

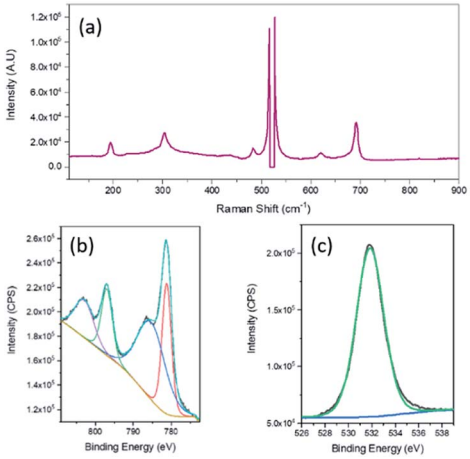

Fig. 3 (a) Raman spectrum, XPS spectra of nanosheets (b) Co 2p and (c) O 1s fabricated from 0.5% Co–GaInSn exposed to 10 mM HCl.

Therefore the use of 10 mM HCl was successful in minimising the formation of gallium oxide while allowing for the oxidation of metallic Co to occur which resulted in the generation of 2D nanosheets of CoO with a thickness of *ca.* 1 nm that contain a significant number of defects and is denoted as CoO_x. This value is consistent with the ultrathin nature of nanosheets that can be produced using a similar approach from metals alloyed with galinstan reported previously that included the much more reactive metals of Gd, Hf and Al which all produced nanosheets less than 1.1 nm in thickness,[21] and Ti with nanosheets of 2 nm thickness.[42] Even though thermodynamically the oxidation of Ga is preferred, as ΔG_f of CoO is much higher at −214.2 kJ mol^{-1}, the presence of 10 mM HCl results in the dissolution of any gallium oxides that are formed which subsequently promotes CoO_x formation. The conditions are also appropriate for the existence of CoO_x in this solution as previous work has shown that CoO only begins to dissolve to a significant extent at concentration of 0.5 M HCl.[43] Therefore the mechanism of formation is due to oxygen bubbles travelling rapidly through the liquid metal causing rapid interfacial oxidation at the air/liquid metal/electrolyte interface due to the Cabrera–Mott oxidation process which limits the growth of the oxide layer at the Co–GaInSn surface to the several Å to nm scale. The nanosheets are then ejected into solution where any Ga_2O_3 that would have formed dissolves allowing for the accumulation of CoO_x nanosheets in solution. The concentration of HCl is enough to dissolve any Ga_2O_3 but allows for CoO_x to exist stably in solution. This will result in some consumption of the Ga component, however the liberated Ga^{3+} ions that are

generated can be in principle be recovered *via* electrochemical reduction to Ga.[44] An advantage of this approach is that it can be done in a single step in a relatively straightforward manner. Other approaches to creating isolated nanosheets of 2D metal oxides require layered materials to be initially synthesised followed by various exfoliation methods which can produce polydispersity in sheet thickness. Another report has shown that indium tin oxide nanosheets can be printed from a liquid InSn alloy held at 200 °C *via* sandwiching the alloy between two substrates which when removed results in ITO nanosheets deposited on the top substrate.[45] The method presented here produces a high proportion of very thin nanosheets in a relatively straightforward process at room temperature.

Electrochemical water splitting in alkaline conditions using various types of cobalt oxides/hydroxides, have been studied previously at a variety of morphologies, including nanosheets, however they have been significantly thicker than reported here at around 6 monolayers per sheet for $Co(OH)_2$.[31] Therefore the 2D CoO_x nanosheets fabricated here were studied for the OER in 0.1 M NaOH. As mentioned previously the effect of the pH of the solution into which the material is ejected is expected to play a critical role. Therefore 1 mM, 10 mM and 50 mM HCl solutions were used to synthesise CoO_x which was then investigated for the OER (Fig. 4a). From this data the material synthesised from 10 mM HCl shows the best performance in terms of current density where values as high as 70 mA cm^{-2} were reached. For the 1 mM HCl solution the formation of gallium oxide is still likely to occur inhibiting the extensive formation of CoO_x while for the 50 mM HCl solution dissolution of CoO_x will be a complicating factor, which results in poor performance due to a lack of material. The amount of Co in the Co–GaInSn mixture was then increased to 1 wt% (Fig. 4b) and 1.5 wt% (Fig. 4c) as a means to increase OER performance. However, in both cases inferior OER current densities were attained compared to 0.5 wt% Co although a slightly better onset potential was achieved for the 1.5 wt% sample. It was also found that the 10 mM HCl solution used in the synthesis was the optimum solution at all weights of Co that was used.

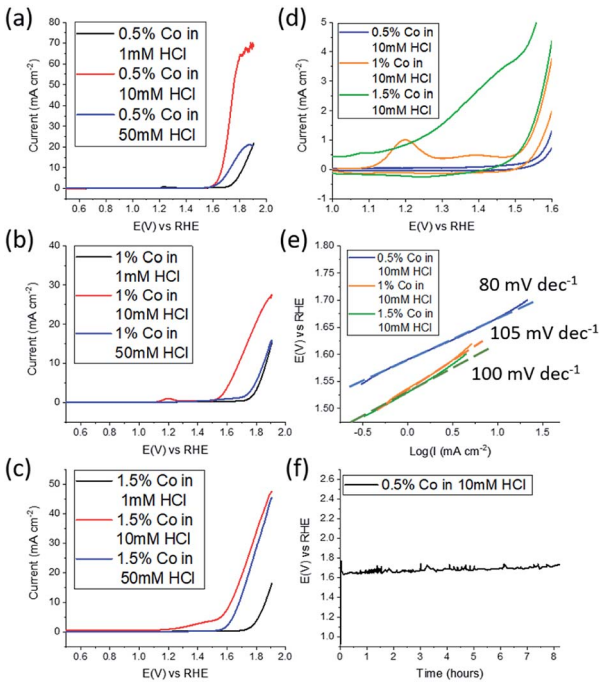

Fig. 4 Linear sweep voltammograms recorded for $Co(OH)_2$/GC in 0.1 M NaOH for the effect of HCl concentration used during the synthesis at (a) 0.5 wt%, (b) 1.0 wt%, (c) 1.5 wt% Co in GaInSn, (d) redox process prior to the OER illustrating the effect of wt% Co, (e) Tafel plots for the OER at different Co concentrations and (f) stability test at 10 mA cm^{-2} for the optimised 0.5 wt% Co–GaInSn sample.

As the 10 mM HCl solution provided the best results, the different weights of Co that were used were compared under these conditions (Fig. 4d). Here the redox processes for CoO_x prior to the onset of the OER are shown. Over the potential range of 1.0 to 1.5 V *vs.* RHE the magnitude of the redox process increases upon increasing the Co content used for the synthesis. The peak that is evident at 1.2 V is due to the oxidation of CoO into CoOOH which is followed by a broader peak at 1.38 V attributed to the oxidation of CoOOH into CoO_2 where the Co^{4+} species is regarded as the active component for the OER.[46,47] From this data it is seen that upon increasing the Co content the magnitude of these redox processes increases prior to the OER, which indicates the formation of more CoO_x, however this does not translate into improved activity.

This is also reflected in the Tafel slope values for the 0.5, 1.0 and 1.5 wt% Co samples which were determined to be 80, 105 and 100 mV dec^{-1} respectively. Therefore, the optimised conditions are gas injection into a Galinstan droplet containing 0.5 wt% Co immersed in a 10 mM HCl solution. It was also found that after 30 min of oxygen gas bubbling that the expulsion of CoO_x nanosheets ceased. The stability of these 2D nanosheets was then investigated at a constant current of 10 mA cm^{-2} where a consistent potential of 1.62 V was maintained for 8 h. This overpotential value of 390 mV is comparable to liquid exfoliated layered $Co(OH)_2$ that was ultrasonicated in aqueous surfactant solution for 4 h which gave an overpotential value of 440 mV.[31] It should be noted that the inherent activity of $Co(OH)_2$ is lower than many other OER electrocatalysts but can be improved by modifying the surface chemistry to carboxylate groups,[48] incorporating S atoms,[49] doping with Fe,[50] adding graphene[51] or gold nanoparticles[32] which provides better activity than reported here. However in terms of the less studied CoO_x material, the performance is slightly better than CoO nanofibers[52] in terms of overpotential at 10 mA cm^{-2} and comparable to previous reports of CoO nanomaterials which were investigated in a more concentrated alkaline electrolyte of 1 M KOH, compared to 0.1 M used here, which gave values of 400 mV for both nanoparticles[53] and nanoplates.[54] Again the activity of CoO can be improved *via* doping with a second metal such as Fe[52] and Zn[54] but this was not the goal of the current study.

Finally, the better performance of the 0.5 wt% Co sample is attributed to the thin nature of the nanosheets that in principle exposes more active sites for the OER. Therefore, to investigate this phenomenon the effect of sheet thickness was investigated. It was found that if the 2D CoO_x nanosheet suspension was allowed to age for 1 week then the thickness of the nanosheets increased to a range of 2.5 to 4 nm as seen from AFM images and the

corresponding histogram for sheet thickness (Fig. S1 and S2†). The electrochemically active surface area (ECSA) was determined using background capacitive measurements (Fig. S3†) where the value decreased by over a factor of 4 from 0.33 mF cm^{-2} to 0.073 mF cm^{-2} which is a result of the increased sheet thickness. This is reflected in a decrease in the OER activity where the OER current density reduced to a value of 25 mA cm^{-2} at 1.70 V (Fig. S4†). This observation is consistent with previous reports showing that increasing the thickness of 2D transition metal oxides decreases electrocatalytic activity.[31]

Conclusions

This study has demonstrated that 2D metal oxide expulsion from the room temperature liquid metal Galinstan is possible even if thermodynamically the formation of gallium oxide is preferred. By controlling the solution pH into which the material is ejected any gallium oxide formed is dissolved allowing for the formation of oxidised Co. Under these conditions the speciation of Co was found to be CoO_x which was ejected into a 10 mM HCl solution in the form of thin 2D nanosheets of *ca.* 1 nm thickness with a length of *ca.* 200 nm. The 2D CoO_x nanosheets were found to be electrocatalytically active for the OER under alkaline conditions to give a current density of 10 mA cm^{-2} at an overpotential of 390 mV with no loss in activity for an electrolysis period of 8 h. It is emphasised here that the goal of this study was not to produce the most active OER electrocatalyst, but to demonstrate a proof of principle that 2D metal oxide nanosheets can be produced that are thermodynamically unfavoured using this simple approach and could be useful for applications other than electrocatalysis. In essence this could be a route to open up many other elements in the periodic table that are difficult to fabricate into nanosheets by taking advantage of the self-limiting oxide formation process that is accessible in room temperature liquid metals.

Conflicts of interest

There are no conflicts to declare.

Notes and references

1 K. Kalantar-Zadeh, J. Tang, T. Daeneke, A. P. O'Mullane, L. A. Stewart, J. Liu, C. Majidi, R. S. Ruoff, P. S. Weiss and M. D. Dickey, *ACS Nano*, 2019, **13**, 7388–7395.
2 Q. Wang, Y. Yu and J. Liu, *Adv. Eng. Mater.*, 2017, **20**, 1700781.
3 T. Daeneke, K. Khoshmanesh, N. Mahmood, I. A. de Castro, D. Esrafilzadeh, S. J. Barrow, M. D. Dickey and K. Kalantar-zadeh, *Chem. Soc. Rev.*, 2018, **47**, 4073–4111.
4 Y. Gao, H. Li and J. Liu, *PLoS One*, 2012, **7**, e45485.
5 M. D. Dickey, *Adv. Mater.*, 2017, **29**, 1606425.
6 H.-J. Koo, J.-H. So, M. D. Dickey and O. D. Velev, *Adv. Mater.*, 2011, **23**, 3559–3564.
7 M. F. Wang, M. J. Jin, X. J. Jin and S. G. Zuo, *Phys. Chem. Chem. Phys.*, 2017, **19**, 18505–18513.
8 K. Khoshmanesh, S.-Y. Tang, J. Y. Zhu, S. Schaefer, A. Mitchell, K. Kalantar-zadeh and M. D. Dickey, *Lab Chip*, 2017, **17**, 974–993.
9 J. Zhang, Y. Yao, L. Sheng and J. Liu, *Adv. Mater.*, 2015, **27**, 2648–2655.
10 S.-Y. Tang, K. Khoshmanesh, V. Sivan, P. Petersen, A. P. O'Mullane, D. Abbott, A. Mitchell and K. Kalantar-zadeh, *Proc. Natl. Acad. Sci. U. S. A.*, 2014, **111**, 3304–3309.
11 S. Holcomb, M. Brothers, A. Diebold, W. Thatcher, D. Mast, C. Tabor and J. Heikenfeld, *Langmuir*, 2016, **32**, 12656–12663.
12 X. Guo, L. Zhang, Y. Ding, J. B. Goodenough and G. Yu, *Energy Environ. Sci.*, 2019, **12**, 2605–2619.
13 F. Hoshyargar, J. Crawford and A. P. O'Mullane, *J. Am. Chem. Soc.*, 2017, **139**, 1464–1471.
14 M. B. Ghasemian, M. Mayyas, S. A. Idrus-Saidi, M. A. Jamal, J. Yang, S. S. Mofarah, E. Adabifiroozjaei, J. Tang, N. Syed, A. P. O'Mullane, T. Daeneke and K. Kalantar-Zadeh, *Adv. Funct. Mater.*, 2019, **29**, 1901649.
15 B. Lertanantawong, P. Lertsathitphong and A. P. O'Mullane, *Electrochem. Commun.*, 2018, **93**, 15–19.
16 C. Zhang, F.-M. Allioux, M. A. Rahim, J. Han, J. Tang, M. B. Ghasemian, S.-Y. Tang, M. Mayyas, T. Daeneke, P. Le-Clech, R. B. Kaner, D. Esrafilzadeh and K. Kalantar-Zadeh, *Chem. Mater.*, 2020, **32**, 4808–4819.
17 Y. Liu, J. Li and W. Zhang, *Chem. Commun.*, 2020, **56**, 6229–6232.
18 J. Ma, Y. Lin, Y.-W. Kim, Y. Ko, J. Kim, K. H. Oh, J.-Y. Sun, C. B. Gorman, M. A. Voinov, A. I. Smirnov, J. Genzer and M. D. Dickey, *ACS Macro Lett.*, 2019, **8**, 1522–1527.
19 M. D. Dickey, *ACS Appl. Mater. Interfaces*, 2014, **6**, 18369–18379.
20 R. A. Robie, B. S. Hemingway and J. R. Fisher, *Thermodynamic properties of minerals and related substances at 298.15 K and 1 bar (105 pascals) pressure and at higher temperatures*, United States Government Printing Office, Washington, 1978.
21 A. Zavabeti, J. Z. Ou, B. J. Carey, N. Syed, R. Orrell-Trigg, E. L. H. Mayes, C. Xu, O. Kavehei, A. P. O'Mullane, R. B. Kaner, K. Kalantar-zadeh and T. Daeneke, *Science*, 2017, **358**, 332–335.
22 I. Roger, M. A. Shipman and M. D. Symes, *Nat. Rev. Chem.*, 2017, **1**, 0003.
23 X. Li, X. Hao, A. Abudula and G. Guan, *J. Mater. Chem. A*, 2016, **4**, 11973–12000.
24 X. Zou and Y. Zhang, *Chem. Soc. Rev.*, 2015, **44**, 5148–5180.
25 N. Cox, D. A. Pantazis, F. Neese and W. Lubitz, *Interface Focus*, 2015, **5**, 20150009.
26 O. M. Anthony Peter, *J. Phys.: Energy*, 2020, DOI: 10.1088/2515-7655/ab8c5f.
27 G. Liu, S. K. Karuturi, A. N. Simonov, M. Fekete, H. Chen, N. Nasiri, N. H. Le, P. Reddy Narangari, M. Lysevych, T. R. Gengenbach, A. Lowe, H. H. Tan, C. Jagadish, L. Spiccia and A. Tricoli, *Adv. Energy Mater.*, 2016, **6**, 1600697.
28 A. Bergmann, E. Martinez-Moreno, D. Teschner, P. Chernev, M. Gliech, J. F. de Araujo, T. Reier, H. Dau and P. Strasser, *Nat. Commun.*, 2015, **6**, 8625.

29 Y.-C. Liu, J. A. Koza and J. A. Switzer, *Electrochim. Acta*, 2014, **140**, 359–365.
30 B. H. R. Suryanto, X. Lu and C. Zhao, *J. Mater. Chem. A*, 2013, **1**, 12726–12731.
31 D. McAteer, I. J. Godwin, Z. Ling, A. Harvey, L. He, C. S. Boland, V. Vega-Mayoral, B. Szydłowska, A. A. Rovetta, C. Backes, J. B. Boland, X. Chen, M. E. G. Lyons and J. N. Coleman, *Adv. Energy Mater.*, 2018, **8**, 1702965.
32 M. A. Sayeed and A. P. O'Mullane, *J. Mater. Chem. A*, 2017, **5**, 23776–23784.
33 B. Lertanantawong, J. D. Riches and A. P. O'Mullane, *Langmuir*, 2018, **34**, 7604–7611.
34 C.-C. Huang and C.-S. Yeh, *New J. Chem.*, 2010, **34**, 103–107.
35 L. S. Reddy, Y. H. Ko and J. S. Yu, *Nanoscale Res. Lett.*, 2015, **10**, 364.
36 P. Benézéth, I. I. Diakonov, G. S. Pokrovski, J.-L. Dandurand, J. Schott and I. L. Khodakovsky, *Geochim. Cosmochim. Acta*, 1997, **61**, 1345–1357.
37 J. S. Gwag and Y.-K. Sohn, *Bull. Korean Chem. Soc.*, 2012, **33**, 505–510.
38 M. M. Alsabban, X. Yang, W. Wahyudi, J.-H. Fu, M. N. Hedhili, J. Ming, C.-W. Yang, M. A. Nadeem, H. Idriss, Z. Lai, L.-J. Li, V. Tung and K.-W. Huang, *ACS Appl. Mater. Interfaces*, 2019, **11**, 20752–20761.
39 H. B. Li, M. H. Yu, X. H. Lu, P. Liu, Y. Liang, J. Xiao, Y. X. Tong and G. W. Yang, *ACS Appl. Mater. Interfaces*, 2014, **6**, 745–749.
40 S. C. Petitto, E. M. Marsh, G. A. Carson and M. A. Langell, *J. Mol. Catal. A: Chem.*, 2008, **281**, 49–58.
41 Y. Tang, L. Dong, S. Mao, H. Gu, T. Malkoske and B. Chen, *ACS Appl. Energy Mater.*, 2018, **1**, 2698–2708.
42 T. Alkathiri, N. Dhar, A. Jannat, N. Syed, M. Mohiuddin, M. M. Y. A. Alsaif, R. S. Datta, K. A. Messalea, B. Y. Zhang, M. W. Khan, A. Elbourne, N. Pillai, J. Z. Ou, A. Zavabeti and T. Daeneke, *Chem. Commun.*, 2020, **56**, 4914–4917.
43 I. Boukerche, N. Habbache, N. Alane, S. Djerad and L. Tifouti, *Ind. Eng. Chem. Res.*, 2010, **49**, 6514–6520.
44 D. O. Flamini, S. B. Saidman and J. B. Bessone, *J. Appl. Electrochem.*, 2007, **37**, 467–471.
45 R. S. Datta, N. Syed, A. Zavabeti, A. Jannat, M. Mohiuddin, M. Rokunuzzaman, B. Yue Zhang, M. A. Rahman, P. Atkin, K. A. Messalea, M. B. Ghasemian, E. D. Gaspera, S. Bhattacharyya, M. S. Fuhrer, S. P. Russo, C. F. McConville, D. Esrafilzadeh, K. Kalantar-Zadeh and T. Daeneke, *Nature Electronics*, 2020, **3**, 51–58.
46 M. A. Sayeed, T. Herd and A. P. O'Mullane, *J. Mater. Chem. A*, 2016, **4**, 991–999.
47 L. D. Burke, M. E. Lyons and O. J. Murphy, *J. Electroanal. Chem. Interfacial Electrochem.*, 1982, **132**, 247–261.
48 C. Qiao, S. Rafai, T. Cao, Z. Wang, H. Wang, Y. Zhu, X. Ma, P. Xu and C. Cao, *ChemCatChem*, 2020, **12**, 2823–2832.
49 H. Zhang, B. Chen, H. Jiang, X. Duan, Y. Zhu and C. Li, *Nanoscale*, 2018, **10**, 12991–12996.
50 M. S. Burke, M. G. Kast, L. Trotochaud, A. M. Smith and S. W. Boettcher, *J. Am. Chem. Soc.*, 2015, **137**, 3638–3648.
51 R. Mehmood, N. Tariq, M. Zaheer, F. Bibi and Z. Iqbal, *Sci. Rep.*, 2018, **8**, 13772.
52 W. Li, M. Li, C. Wang, Y. Wei and X. Lu, *Appl. Surf. Sci.*, 2020, **506**, 144680.
53 Z.-J. Jiang and Z. Jiang, *Sci. Rep.*, 2016, **6**, 27081.
54 M. Huo, Z. Yang, C. Yang, Z. Gao, J. Qi, Z. Liang, K. Liu, H. Chen, H. Zheng and R. Cao, *ChemCatChem*, 2019, **11**, 1480–1486.

